Atmos. Meas. Tech. Discuss., 4, 2567–2598, 2011
www.atmos-meas-tech-discuss.net/4/2567/2011/
doi:10.5194/amtd-4-2567-2011

Atmospheric Measurement Techniques Discussions

Volcanic ash detection and retrievals from MODIS data by means of Neural Networks

M. Picchiani[1], M. Chini[2], S. Corradini[2], L. Merucci[2], P. Sellitto[3], F. Del Frate[1], and S. Stramondo[2]

[1]Earth Observation Laboratory, Tor Vergata University, Rome, Italy
[2]Istituto Nazionale di Geofisica e Vulcanologia, Rome, Italy
[3]Laboratoire Inter-universitaire des Systèmes Atmosphériques (LISA), UMR7583, CNRS – Universités Paris-Est et Paris Diderot, Créteil, France

Received: 11 April 2011 – Accepted: 22 April 2011 – Published: 4 May 2011

Correspondence to: M. Picchiani (picchian@disp.uniroma2.it)

Published by Copernicus Publications on behalf of the European Geosciences Union.

Abstract

Volcanic ash clouds detection and retrieval represent a key issue for the aviation safety due to the harming effects they can provoke on aircrafts. A lesson learned from the recent Icelandic Eyjafjalla volcano eruption is the need to obtain accurate and reliable retrievals on a real time basis.

The current most widely adopted procedures for ash detection and retrieval are based on the Brightness Temperature Difference (BTD) inversion observed at 11 and 12 µm that allows volcanic and meteo clouds discrimination. While ash cloud detection can be readily obtained, a reliable quantitative ash cloud retrieval can be so time consuming to prevent its utilization during the crisis phase.

In this work a fast and accurate Neural Network (NN) approach to detect and retrieve volcanic ash cloud properties has been developed using multispectral IR measurements collected by the Moderate Resolution Imaging Spectroradiometer (MODIS) over Mt. Etna volcano during 2001, 2002 and 2006 eruptive events.

The procedure consists in two separate steps: the ash detection and ash mass retrieval. The detection is reduced to a classification problem by identifying two classes of "ashy" and "non-ashy" pixels in the MODIS images. Then the ash mass is estimated by means of the NN, replicating the BTD-based model performances.

The results obtained from the entire procedure are very encouraging; indeed the confusion matrix for the test set has an accuracy greater than 90 %. Both ash detection and retrieval show a good agreement when compared to the results achieved by the BTD-based procedure. Moreover, the NN procedure is so fast to be extremely attractive in all the cases when the quick response time of the system is a mandatory requirement.

AMTD

4, 2567–2598, 2011

1 Introduction

The recent Eyjafjalla eruption showed clearly that real time detection and tracking of the volcanic cloud evolution based on satellite data plays a key role in the aviation crisis management. Because of the well known harming effects of ash cloud particles on aircrafts (loss of power, failure of high-bypass turbine engines, abrasion of turbine blades, windscreens, fuselage, and Pitot static tubes, see Miller and Casadevall, 2000, many European airports were closed causing millions of passengers to be stranded, with a worldwide airline industry loss estimated of about 2.5 billion Euros (EUMETSAT Report, 2010). Both security and economical grounds necessitate a great effort to realize reliable and robust ash cloud detection and retrieval on a real time basis.

Because of the sporadic nature and the large spatial extent of the volcanic ash clouds, satellite remote sensing represents the most suitable tool to attack the problem. The best known approach to detect and retrieve volcanic ash is based on the BTD of two channels centered on 11 and 12 µm. The inversion observed in the BTD behavior when evaluated on meteorological and volcanic clouds, the underlying microphysical model and the accurate satellite data simulation by means of radiative transfer codes are the main foundations of this method (Prata, 1989a; Wen and Rose, 1994). The technique has been applied either to polar satellite instruments as the Advanced Very High Resolution Radiometer (AVHRR) (Prata, 1989b; Wen and Rose, 1994), the Moderate Resolution Imaging Spectroradiometer (MODIS) (Hillger et al., 2002; Watson et al., 2004; Tupper at al., 2004; Corradini et al., 2008a, 2010, 2011), than to geostationary satellite instruments as the Geostationary Operational Environmental Satellite (GOES) (Yu et al., 2002), and the Spin Enhanced Visible and Infrared Imager (SEVIRI) measurements (Prata and Kerkmann, 2007; Corradini et al., 2008b). The use of radiative transfer models for the ash retrievals has two main drawbacks: the need of several inputs and the processing time. The latter can yield to time consuming retrievals that can prevent an effective utilization of this information during the crisis phases.

Since the beginning of the 1990s the Neural Networks (NNs) (Lippmann, 1987) have been exploited to analyze remote sensing data (Atkinson and Tatnall, 1997; Mas and Flores 2008). Several authors have highlighted the effectiveness of the NNs in the observation of the Earth's environment from space. The universal approximator capability (Krasnopolsky et al., 1995) as well as the independence from a priori constrains about the data distributions (Civco 1993; Benediktsson and Sveinsson, 1997; Carpenter et al., 1997) represent two of the most attractive advantages of NNs with respect to other inversion algorithms. Furthermore NNs are able to positively combine different type of input data, i.e. data acquired from different sensors (Benediktsson et al., 1993; Chini et al., 2009; Pacifici et al., 2009), as well as to incorporate a priori knowledge and realistic physical constraints into the analysis (Foody 1995a, b), properties of great interest for remote sensing applications. The comparison of statistical classification methods and NNs has shown that NNs can achieve better accuracies (Benediktsson et al., 1990, 1993; Chini et al., 2008). In the field of the atmospheric investigations the NNs have been successfully used to address different problems such as: humidity profiles retrieval (Cabrera-Mercader and Staelin 1995; Blackwell, 2005), height resolved ozone retrievals (Del Frate and Schiavon, 1999; Del Frate et al., 2002; Müller et al., 2003; Sellitto et al., 2011a, b), cloud classification (Lee et al., 1990; Bankert, 1994), temperature parameter estimates (Butler, et al., 1996) and retrieval of temperature profiles (Churnside et al., 1994).

In this work we present an innovative approach in which the capability of the NNs is exploited to obtain accurate near real time volcanic ash clouds' detection and retrieval in order to sample the phenomenon evolution. In particular, we highlight that in a NNs based algorithm the time cost is transferred to the preliminary training phase, thus allowing processing the satellite images in quasi real time.

2 MODIS instrument

The MODerate resolution Imager Spectroradiometer (MODIS) is a multi-spectral instrument aboard on the Earth Observing System (EOS) Terra and Aqua satellites (Barnes et al., 1998; http://modis.gsfc.nasa.gov/). The two satellites have different equatorial crossing times: Terra is characterized by a morning overpass, while Aqua by an afternoon one, with a global coverage in 1 or 2 days. MODIS covers 36 spectral bands, from visible (VIS) to thermal infrared (TIR), and a spatial resolution that varies from 250 m to 1000 m, depending on the acquisition mode. A summary of the TIR channels characteristics is given in Table 1.

In the present work the bands 31 and 32 have been used for the volcanic ash detection and retrievals by using the Brightness Temperature Difference (BTD) procedure (see Sect. 4). In the NNs approach (see Sect. 5) the band 28 is also used to account for the atmospheric water vapor effect on ash detection (Corradini et al., 2008a).

3 Test Cases

Mt. Etna volcano (37.73° N, 15.00° E) is a massive stratovolcano (3330 m a.s.l.) located in the eastern part of Sicily (Italy). With a summit elevation of 3315 m, is the largest and most active European volcano and one of the major degassing volcanoes worldwide. Its eruptive activity occurs nearly every year both at the summit four craters and on the flanks.

During the eruptions significant emissions of gases and ash can be injected into the atmosphere. Ash fallout periodically reaches the surrounding areas affecting the local population and disrupting the nearby Catania, Sigonella, and Reggio Calabria airports activities.

In this work five MODIS images, collected during the 2001 (23 July, at 10:35 UTC), 2002 (28, 29 and 30 October at 12:15, 9:45 and 12:05 UTC respectively) and 2006

AMTD
4, 2567–2598, 2011

(24 November at 12:20 UTC) Mt. Etna eruptions, have been considered as test cases. Figure 1 shows the channel 31 of five MODIS images affected by the ash absorption.

The considered MODIS dataset is representative of different volcano eruption typologies (high and medium ash emissions) occurred during different seasons (spring, autumn and winter).

4 Brightness Temperature Difference procedure description

The Brightness Temperature Description (BTD) procedure used for the volcanic ash detection, exploiting the selective absorption in the TIR spectral range, is based on the difference between the brightness temperatures of two TIR channels centered on 11 and 12 µm (Prata, 1989a, b). The main BTD advantage is its very simple and fast application, while the main drawbacks are the false alarms (negative and positive ash detections) obtained in specific and well documented cases (Simpson et al., 2000; Prata et al., 2001; Simpson et al., 2001), as over clear land surfaces at night (Platt and Prata, 1993), over soils with a high quartz content (e.g., deserts) (Barton and Takashima, 1986), over very cold surfaces (temperatures less than 220 K) (Potts and Ebert, 1996), over ice-covered surfaces (Yamanouchi et al., 1987) and in presence of high water vapour content (Prata et al., 2001; Yu et al., 2002; Corradini et al., 2008a). This latter effect, that tends to attenuate and in some cases can completely cancel-out the BTD signal, has been corrected by applying a procedure developed by Corradini et al. (2008a). The ash mass is computed in each pixel by using the simplified formula suggested by Wen and Rose (1994) exploiting the ash density, the pixel size, the ash extinction efficiency factor and the effective radius (r_e) and optical depth (τ), where r_e and τ are obtained from the Top Of Atmosphere (TOA) simulated "inverted arches" BTD curves vs. brightness temperature at 11 µm (Wen and Rose, 1994; Prata and Grant, 2001; Yu et al., 2002).

The simulated TOA radiances Look-Up Table (LUT) needed for the ash retrievals are computed by using the MODTRAN 4 (Berk et al., 1989; Anderson et al., 1995)

Radiative Transfer Model (RTM). The inputs to MODTRAN are the atmospheric profiles of Pressure, Temperature and Humidity (PTH), the surface characteristics (temperature and emissivity), the volcanic plume altitude and thickness, and the volcanic ash optical properties. In this work all the atmospheric profiles have been collected at the Trapani WMO Meteo Station (the meteorological station nearest to the volcanic area). In all the cases considered in this study the ash clouds were mainly located over the sea; therefore the surface emissivity has been taken equal to 0.99 for both 11 and 12 µm channels. The surface temperature is computed by inverting the radiative transfer equation in the TIR spectral range. The volcanic cloud altitude has been derived from the comparison between the 11 µm brightness temperature of the ash cloud most opaque pixels and the WMO atmospheric temperature profiles (see Prata and Grant, 2001; Corradini et al., 2008a). The ash optical properties are derived using a Mie code (EODG, Oxford University) using the Volz et al. (1973) refractive index. The density of ash has been set to $2.6 \times 10^6\,\mathrm{g\,m^{-3}}$ (Neal et al., 1994). The final set of RTM simulations, computed in a multiple scattering atmosphere (16 streams), uses 801 wavelengths (from 700 to 1500 $\mathrm{cm^{-1}}$, step 1 $\mathrm{cm^{-1}}$ × 15 angles (from 0 to 75°, step 5°) × 9 optical depths (from 0 to 10, constant step in a logarithmic scale) × 8 particle effective radii (from 0.4 to 10 mm, constant step in a logarithmic scale). The total computational time for each LUT, by considering a personal computer (Intel dual core processor 2, 13 GHz) is about 4 h.

Every MODTRAN input parameter has an uncertainty that will cause errors in the ash retrievals. A 40 % of total ash mass retrieval error has been considered, accordingly to the sensitivity study carried out by Corradini et al. (2008a) considering the uncertainties of many parameters such as atmospheric profiles, plume geometry, surface temperature and emissivity and ash type.

4.1 Ash Mass retrievals results

In Figs. 2 and 3 we show the ash detection and retrieval maps, respectively, computed by means of the BTD procedure applied to the 5 MODIS test case measurements.

The retrievals show the huge amount of ash emitted during the 2001 and 2002 eruption events, affecting the south Mediterranean area and north Africa. The 2006 ash emission was significantly lower, limiting the problems to the Etna surrounding area and to the Catania Fontanarossa airport.

5 Neural Network approach

In this section the Neural Network (NN) methodology for the ash detection and retrieval is described. The first problem handled is the identification of volcanic ash, while the second one is the retrieval of the ash total mass only where ash has been detected. For the two cases two separate NNs have been used. As it has already been mentioned, the most effective set of channels from MODIS sensor have been considered as input for both NNs, which are the channel 28, 31 and 32 (hereafter CH28, CH31 and CH32).

The NNs are statistical-mathematical models designed to extract the underlying relationships between a given number of input and output quantities. In this work we have considered a particular type of NNs known as feed-forward multilayer perceptron (MLP) (Bishop, 1995; Haykin, 1994). MLP-NNs are composed of elementary computational units called neurons, organized in layers. Usually we have one Input layer, one Output layer and one or more Hidden layers (Funahashi, 1989). The elements of each layer are connected to the elements of adjacent layers with weighted links, and the signal propagates from one layer to the next only along the input-output (forward) direction. Each neuron accepts as input a combination of the outputs from the neurons of the previous layer, and processes it by means of its Activation Function (AF). The learning stage is performed by the progressive and iterative adjustment of the weights, in order to minimize the error, between the outputs computed by the NN and the known true outputs, on an appropriate set of input-output training samples, also called training patterns. During the training phase, a trade-off between accuracy and generalization capabilities of the networks is reached when the error function on an independent set of patterns, also called test set, reaches the global minimum (Prechelt, 1998). It has

AMTD
4, 2567–2598, 2011

been demonstrated that any continuous mapping can be approximated to whatever accuracy by an MLP, with at least a hidden layer and a sufficient number of hidden neurons with sigmoidal activation function (Cybenko, 1989; Hornik et al., 1989). Moreover, in Gardner and Dorling (1998) and in Hsieh and Tang (1998) is shown how the use of this kind of NNs it is effective for the solution of atmospheric inverse problems that involve complex physical behaviors.

Relying on their capability of discovering appropriate functional mapping between the inputs and the outputs spaces, we have used the MLP-NN to approximate the linking function between the measured quantity, i.e. brightness temperature, and the quantity of interest, like the presence of ash and its mass. Furthermore, once the NN is correctly trained, it can process the new data in quasi real time thanks to its high speed computation (Del Frate et al., 2002). This opportunity makes the inversion method based on NN algorithm very attractive when the computation time speed is a concern.

As target output we have considered the results obtained by the BTD procedure over a fixed number of MODIS images.

5.1 NNs for volcanic ash detection

The first problem is the identification of volcanic ash using MODIS data. The input space is composed of three MODIS channels such as CH28, CH31 and CH32. The last two channels are the same considered for the BTD procedure. We observe that the BTD procedure also uses other ancillary data that are not taken into account in the NN algorithm. In the BTD algorithm the atmospheric water vapor correction is computed to improve the detection of the ash. This is achieved using the atmospheric profile derived from ground meteorological station. Differently, in the NN architecture the water vapor content is taken into account adding as input to the network the CH28. It is worth to note that CH28 is centered around 7.3 µm, where the atmospheric water vapor absorption is particularly strong. Concerning the outputs, we configured the ash detection as a classification problem, where the output space is divided in two classes such as *Ash* and *No Ash* (hereafter *A* and *NA*). This latter is clearly a simplification, as many other possible classes, e.g. meteorological clouds, have not been considered.

To generate the training set (*TrS*) and the test set (*TeS*) we chose the acquisition of 28 October 2002 and of 29 October 2002, while the data collected on 23 July 2001, 30 October 2002 and 24 November 2006, have been used for evaluating the classification performance. This approach has been considered in order to assess the generalization capabilities of the NN and the statistical representativeness of the training/test samples. Considering the histograms of the measurements at the three channels and of the estimates of the ash mass computed by the BTD procedure (Fig. 4), it is possible to observe that the 28 October 2002 and of 29 October 2002, have a more exhaustive data distribution; this behavior has guided the choice of the two dates for the *TrS* and *TeS*.

The input-output samples of the *TrS* and *TeS* have been created matching the CH28, CH31 and CH32 data with the ash map obtained by the BTD procedure, which is the target output (see Fig. 2). Based on the target output map, we have randomly extracted a number n of pixels for *A* and an equal number for *NA* classes in order to have a balanced *TrS*. The *TeS* is obtained similarly by the selection of m independent pixels ($m < n$).

5.2 NNs for volcanic ash mass retrieval

The second issue is the retrieval of the total mass of the ash. The input dataset of the NN is the same as for the ash detection, i.e. CH28, CH31 and CH32, while the output is the ash mass (tons km^{-2}). Differently from the detection, which is a classification exercise, the network performs an estimation of a physical parameter, replicating the BTD model. Therefore the BTD model results (shown in Fig. 3) have been used to extract the target output information to the NN.

The training/test and validation phases are completely focused on the target output regions where the ash plume is identified, according to the BTD ash detection maps (see Fig. 2). Since more than one MODIS image representative of the different events

AMTD
4, 2567–2598, 2011

is available, a study on the generalization capability of the NN is possible, as explained in the following.

For each date i three separate independent subsets have been generated: a training set (TrS_i), a test set (TeS_i) and a validation set (VaS_i), with i, spanning from 1 to p, and p being the total amount of acquisitions. Different NNs have been trained with an increasing number of samples. In particular, starting with $i = 1$, the NN at stage $i + 1$ is obtained by adding to TrS_i the elements belonging to TrS_{i+1} . At each step the performance of the retrieval has been tested on all p VaS. It is worth noting that at all p-1 stages there is at least one validation test whose samples belong to an image not considered in the training phase. The results expected by this approach are an improvement of the ash mass retrieval performance with the increase of the training samples taken from completely uncorrelated acquisitions. In fact, the inclusion of additional samples should provide a better statistical representation of the phenomenon. This hypothesis will be validated in the Sect. 6.2 where the results for the different VaS_i sets, obtained by means of the different NN_i, are shown.

6 Experimental results

In this section we present the results obtained applying the proposed procedures for the ash cloud detection and the retrieval of the ash cloud mass. First the NNs-based ash detection is compared with the results obtained applied the BTD procedure, and then the performance of the NNs retrieval results is shown and discussed.

6.1 Ash detection results

As explained in Sect. 5.2 the problem of the ash detection can be addressed as a classification exercise considering two classes, A and NA, with TrS and TeS randomly extracted from the 28 October 2002 and 29 October 2002 acquisition dates, while the

AMTD
4, 2567–2598, 2011

remaining dates have been used for the validation phase. In Table 2 the patterns forming *TrS*, *TeS* and *VaS*, extracted for each acquisition date are shown.

The NN has been trained with a *TrS* and a *TeS*, composed by 56334 and 24414 patterns respectively, extracted from 28–29 October 2002 acquisitions. Each independent VaS, extracted from the remaining data, is composed by 810000 patterns. After a phase where different NN topologies have been tested, we have selected the topology with the minimum complexity giving the best performance. The identified NN is a MLP with a single hidden layer, a sigmoidal activation function for the units, and the following topology: [3]–[10]–[2].

Figure 5a shows the results of the NN classification procedure applied to all the MODIS measurements. The ash clouds are well recognized and characterized, indeed the comparison with the ash detection carried out by means of BTD technique (see Fig. 2) indicates a very good agreement. Figure 5a shows also some false positive ash detection since, in the considered channels, the high meteorological clouds exhibit a similar spectral behavior of the ash cloud (see Sect. 4). To avoid these errors, an object-oriented approach has been applied. In particular we considered the pixel corresponding to the volcano's vent as the seed for a region growing algorithm. In this way the resulting ash map is composed by the closest object to the volcano vent while all originally detected areas far from the volcano vent, hence very likely corresponding to false alarms, are removed (Pulvirenti et al., 2011).

Figure 5b shows the results of the object-oriented procedure. Among the elimination of the false positives, the figure displays also the disappearance of some parts of the ash cloud in its distal part (see for example the 23 July 2001 image). Such expected effect restrict the use of the segmentation procedure to cases where the volcanic emission is continuous, when we are interested to analyze the ash cloud impact on the area surrounding the volcano or when we want to focus our study on the volcanic emission processes. The classification accuracy has also been quantitatively analyzed by confusion matrixes, computed with and without the region growing step (see Table 4). Both, the overall accuracy and the K coefficient parameters confirm that the results obtained by the developed NN procedure are in agreement with the results obtained by the BTD procedure. Moreover, the post classification segmentation procedure slightly increases the classification accuracies (see right column of Table 4).

6.2 Ash mass retrieval results

The approach used for the ash mass retrieval from the CH28, CH31, and CH32 has already been explained in Sect. 5.3. In Table 5 the number of patterns extracted from the different acquisition dates for the *TrS*, *TeS* and *VaS* are reported. The adopted network topology is the same of the ash detection, except for the output layer which consists of a single neuron, i.e. [3]–[10]–[1].

To investigate further the relation between the statistical representativeness of the data used in the training phase and the NN retrieval accuracy, an ensemble of scatter plots for the five *V* sets has been computed and is shown in Fig. 6. The results, for the *VaS* extracted from the all five dates, reached with the NN trained only with the patterns from the 28 October 2002 are shown on top of the figure. The successive scatter plots, arranged in rows, show the results obtained adding training set data from a successive acquisition. For instance, in the second row are shown the scatter plots for all five *VaS* as well, while the training and test sets have been obtained joining the *TrS* and *TeS* of the data taken on 28 October 2002 and 29 October 2002 and so on for the others rows. The results are less easily interpretable than those obtained for the ash detection, therefore a brief comment seems appropriate in evaluating the effectiveness of the proposed method. The first evidence is that the retrieval results are already positive with the NN trained only with the *TrS* and *TeS* extracted from the first acquired date (28 October 2002). This is probably due to the large number of patterns considered in the first training set. For the majority of the input-output patterns of the other four *VaS* the statistical representativeness of the *TrS* seems to be appropriate (see Fig. 4). In fact the Pearson correlation coefficients between the true and the retrieved parameters are always major or equal to 0.95 (see the first row of Fig. 6), while the slope of the regression line it is closer to one with the increase of

AMTD
4, 2567–2598, 2011

the training/test patterns from different date. The latter is indeed an important indicator for evaluating the ash mass retrieval capability of the NN (see Fig. 6), because when the number of training patterns increases an improvement of the parameter can be observed.

The above analysis seems to uphold the effectiveness of the proposed approach: when increasing the training data, an increase of the retrieval accuracy can be appreciated. This tendency can be evaluated from the ensemble of scatter plots shown in Fig. 6, as well as considering the trend of the rmse values for the five *VaS* sets obtained by means of the five different NNs (see Table 6).

Considering the evidences discussed above for computing the ash total mass maps we have adopted the NN5, trained with the total training set. The retrieved ash mass maps are shown in Fig. 7. The retrieval has been done only where the ash has been detected by the NN detection algorithm with region growing algorithm previously described. The visual analysis of the maps confirms the positive results obtained with the proposed approach. In particular the comparison of BTD (see Fig. 3) and NN (see Fig. 7) results shows very similar concentration (i.e. colours) and shape features, thus evidencing the ability of the NN algorithm to approximate the results provided by the BTD MODTRAN-based method.

7 Conclusions

In this work a NN procedure for detecting volcanic ash clouds and retrieving the ash clouds' mass has been implemented and discussed. The considered test cases are several eruptions of Mt. Etna volcano occurred in 2001, 2002 and 2006 and imaged by MODIS instrument. It has been shown that the neural approach drastically reduces the computational burden required for the data processing. Indeed, the ash cloud detection and the production of the ash clouds' mass maps are produced in few minutes. This is a much shorter time if compared with the several hours usually needed using a more traditional LUT based approach. The described technique is therefore

AMTD
4, 2567–2598, 2011

extremely attractive during a crisis phase, when a fast development of the results is a mandatory requirement. On the other hand, the improvement in the processing time is achieved without lowering the accuracies characterizing the estimated quantities. Once the learning phase is over, when tested on data not belonging to the training set, the NN provides results in good agreement with the those given by the BTD-based technique. This is true for both the ash detection and the mass retrieval cases. In particular the detected ash maps have a mean K-coefficient around 0.8, while the regression curves of the ash mass retrievals have an rmse close to 0.3. An object-oriented approach has also been applied to avoid the false positive ash pixels detected by the technique and induced by the presence of high meteorological clouds. The comparison with the ground truth shows that, even if yields a benefit in terms of classification accuracy, the segmentation procedure also eliminates actual ash clouds appearing in the distal part. This latter effect limits the use of the procedure only in the particular cases where the volcanic emission is continuous, thus when we are interested to analyze the ash cloud impact on the area surrounding the volcano or when we want to focus our study on the volcanic emission processes.

It must be stressed that the proposed inversion scheme can be easily extended in order to consider additional bands, hence to make more information available as input. In fact, future improvements include the use of visible and near infrared channels for meteorological clouds detection, and the retrieval of the ash cloud optical depth and effective radius. The generalization capabilities of the NN in this field is another aspect that can be more deeply investigated by considering different volcanic eruptions in time, as well for different test sites.

Acknowledgements. S. Corradinis work was supported by the European Space Agency SAVAA (Support to Aviation Services for Volcanic Ash Avoidance) project.

References

Anderson, G. P., Wang, J., and Chrtwynd, J. H.: MODTRAN3: An update and recent validation against airborne high resolution inferometer measurements, In Summaries of the Fifth Annual Jet Propulsion Laboratory Airborne Earth Science Workshop, 95–1(1), 5–8, 1995.

Atkinson, P. M. and Tatnall, A. R. L.: Neural networks in remote sensing, Int. J. Remote Sens., 18, 699–709, 1997.

Bankert, R. L.: Cloud classification of AVHRR imagery in maritime regions using a probabilistic neural network, J. Appl. Meteorol., 33, 909–918, 1994.

Barnes, W. L., Pagano, T. S., and Salomonson, V. V.: Prelaunch characteristics of the Moderate Resolution Imaging Spectroradiometer (MODIS) on EOS-AMI, IEEE T. Geosci. Remote, 36, 1088–1100, 1998.

Barton, I. J. and Takashima, T.: An AVHRR investigation of surface emissivity near Lake Eyre, Australia, Remote Sens. Environ., 20, 153– 163, 1986.

Benediktsson, J. A., Swain, P. H., and Ersoy, O. K.: Neural network approaches versus statistical methods in classification of multisource remote sensing data, Int. J. Remote Sens., 28, 540–552, 1990.

Benediktsson, J. A., Swain, P. H., and Esroy, O. K.: Conjugate-gradient neural networks in classification of multisource and very-high-dimensional remote sensing data, Int. J. Remote Sens., 14, 2883–2903, 1993.

Benediktsson, J. A. and Sveinsson, J. R.: Feature extraction for multisource data classification with artificial neural networks, Int. J. Remote Sens., 18, 727–740, 1997.

Berk, A., Bernstein, L. S., Anderson, G. P., Acharya, P. K., Robertson, D. C., Chetwynd, J. H., and Adler-Golden, S. M.: Modtran cloud and multiple scattering upgrades with application to AVIRIS, Remote Sens. Environ., 65, 367–375, 1998.

Bishop, C. M.: Neural Networks for Pattern Recognition, Oxford University Press, 1995.

Blackwell, W. J.: A neural-network technique for the retrieval of atmospheric temperature and moisture profiles from high spectral resolution sounding data, IEEE T. Geosci. Remote, 43, 2535–2546, 2005.

Butler, C. T., Meredith, R. V. Z., and Stogryn, A. P.: Retrieving atmospheric temperature parameters from DMSP SSM/T-1 data with a neural network, J. Geophys. Res., 101(D3), 7075–7083, 1996.

Cabrera-Mercader, C. R. and Staelin, D. H.: Passive microwave relative humidity retrievals

using feed forward neural networks, IEEE T. Geosci. Remote, 33, 1324–1328, 1995.
Carpenter, G. A., Gjaja, M. N., Gopal, S., and Woodcock, C. E.: ART neural networks for remote sensing: vegetation classification from Landsat TM and terrain data, IEEE T. Geosci. Remote, 35, 308–325, 1997.
Churnside, J. H., Stermitz, T. A., and Schroeder, J. A.: Temperature profiling with neural network inversion of microwave radiometer data, J. Atmos. Oceanic Technol., 11, 105–109, 1994.
Chini, M., Pacifici, F., Emery, W. J., Pierdicca, N., and Del Frate, F: Comparing Statistical and Neural Network Methods Applied to Very High Resolution Satellite Images Showing Changes in Man-Made Structures at Rocky Flats, IEEE T. Geosci. Remote, 46(6), 1812–1821, 2008.
Chini, M., Pacifici, F., and Emery, W. J.: Morphological operators applied to X – band SAR for urban land use classification, Proc. IEEE/IGARSS 2009, IV 506 – IV 509, 2009.
Civco, D. L.: Artificial neural networks for land-cover classification and mapping, Int. J. Geogr. Inf. Syst., 7, 173–186, 1993.
Corradini, S., Spinetti, C., Carboni, E., Tirelli, C., Buongiorno, M. F., Pugnaghi, S., and Gangale, G.: Mt. Etna tropospheric ash retrieval and sensitivity analysis using Moderate Resolution Imaging Spectroradiometer measurements, J. Appl. Rem. Sens., 2, 023550, doi:10.1117/1.3046674, 2008a.
Corradini, S., Merucci, L., Prata, F., Silvestri, M., Musacchio, M., Spinetti, C., Piscini, A., and Buongiorno, M. F.: SO_2 and ash plume retrievals using MSG-SEVIRI measurements. Test case: 24 November 2006 Mt. Etna eruption, IEEE USEREST Workshop, Naples 11–14 November, 2008b.
Corradini, S., Merucci, L., Prata, A. J., and Piscini, A.: Volcanic ash and SO2 in the 2008 Kasatochi eruption: Retrievals comparison from different IR satellite sensors, J. Geophys. Res., 115, D00L21, doi:10.1029/2009JD013634, 2010.
Corradini, S., Merucci, L., and Arnau, F.: Volcanic ash cloud properties: comparison between MODIS satellite retrievals and FALL3D transport model, IEEE Geosci. Remote S., 8 (2), 248–252, 2011.
Cybenko, G.: Approximation by superpositions of a sigmoidal function, Math. Control, Signals, Syst., 2, 303–314, 1989.
Del Frate, F. and Schiavon, G.: Nonlinear principal component analysis for the radiometric inversion of atmospheric profiles by using neural networks, IEEE T. Geosci. Remote, 37, 2335–2342, 1999.

Del Frate, F., Ortenzi, A., Casadio, S., and Zehner, C.: Application of neural algorithms for a real-time estimation of ozone profiles from GOME measurements", IEEE T. Geosci. Remote, 40(10), 2263–2270, 2002.
EUMETSAT Report: Monitoring volcanic ash from space ESA-EUMETSAT workshop on the 14 April to 23 May 2010 eruption at the Eyjafjöll volcano, South Iceland, C. Zehner (Editor) ESA/ESRIN, May 26–27, http://earth.eo.esa.int/workshops/Volcano/files/STM-280_ash101004_V2.pdf, 2010.
Foody, G. M.: Using prior knowledge in artificial neural network classification with a minimal training set, Int. J. Remote Sens., 16, 301–312, 1995a.
Foody, G. M.: Land cover classification using an artificial neural network with ancillary information, Int. J. Geogr. Inf. Syst., 9, 527–542, 1995b.
Funahashi, K.: On the approximate realization of continuous mappings by neural net-works, Neural Networks, 2, 183–192, 1989.
Gardner, M. W. and Dorling, S. R.: Artificial neural networks (the multilayer perceptron) – A review of applications in the atmospheric sciences, Atmos. Environ., 32, 2627–2636, 1998.
Haykin, S.: Neural Networks: A Comprehensive Foundation, Macmillan, New York, 1994.
Hillger, D. W. and Clark, J. D.: Principal component image analysis of MODIS for volcanic ash. Part I: Most Important Bands and Implications for Future GOES Imagers, J. Appl. Meteorol., 41(10), 985–1001, 2002.
Hornik, K. M., Stinchcombe, M., and White, H: Multilayer feedforward networks are universal approximators, Neural Networks, 2, 359–366, 1989.
Hsieh, W. W. and Tang, B.: Applying neural network models to prediction and data analysis in meteorology and oceanography, Bull. Am. Meteorol. Soc., 79, 1855–1870, 1998.
Krasnopolsky, V. M., Breaker, L. C., and Gemmill, W H.: A neural network as a nonlinear transfer function model for retrieving surface wind speeds from the special sensor microwave imager, J. Geophys. Res., 100, 11033–11045, 1995.
Lee, J., Weger, R. C., Sengupta, S. K., and Welch, R. M.: A neural network approach to cloud classification, IEEE T. Geosci. Remote, 28, 846–855, 1990.
Lippmann, R.: An introduction to computing with neural nets, IEEE ASSP Magazine, 4, 4–22, 1987.
Mas, J. F. and Flores, J. J.: The application of artificial neural networks to the analysis of remotely sensed data, Int. J. Remote Sens., 29, 617–663, 2008.
Miller, T. P. and Casadevall, T. J.: Volcanic Ash Hazards to Aviation, Encyclopedia of Volcanoes,

edited by: Sigurdsson, H., Academic Press, San Diego, California, 915–930, 2000.
Müller, M. D., Kaifel, A. K., Weber, M., Tellmann, S., Burrows, J. P., and Loyola, D.: Ozone profile retrieval from Global Ozone Monitoring Experiment (GOME) data using a neural network approach (Neural Network Ozone Retrieval System (NNORSY)), J. Geophys. Res., 108, 4497, doi:10.1029/2002JD002784, 2003.
Neal, C. A., Mc Gimsey, R. G., Gardner, C. A., Harbin, M. L., and Nye, C. J.: Tephra-fall from 1992 eruptions of Crater Peak, Mount Spurr Volcano, AK: A preliminary report on distribution, stratigraphy and composition, in: Keith TEC (ed) The 1992 eruptions of Crater Peak vent, Mount Spurr Volcano, Alaska, US Geol. Surv. Bull., 2139, 65–79, 1994.
Oxford University, Atmospheric Oceanic and Planetary Physics Dept., EODG group Mie Code: Light scattering routines, http://www.atm.ox.ac.uk/code/mie/index.html,2006.
Pacifici, F., Chini, M., and Emery, W. J.: A neural network approach using multi-scale textural metrics from very high resolution panchromatic imagery for urban land-use classification, Remote Sens. Environ., 113(6), 1276–1292, 2009.
Platt, C. M. R. and Prata, A. J.: Nocturnal effects in the retrieval of land surface temperatures from satellite measurements, Remote Sens. Environ., 45, 127–136, 1993.
Potts, R. J. and Ebert, E. E.: On the detection of volcanic ash in NOAA AVHRR infrared satellite imagery, in: 8th Australian remote sensing conference, Canberra (25–29). Floreat, Western Australia, Remote Sensing and Photogrammetry Association Australia (March), 1996.
Prata, A. J.: Infrared radiative transfer calculations for volcanic ash clouds, Geoph. Res. Lett., 16(11), 1293–1296, 1989a.
Prata, A. J.: Observation of volcanic ash clouds using AVHRR-2 radiances, Int. J. Rem. Sens., 10(4), 751–761, 1989b.
Prata, A. J. and Grant, I. F.: Determination of mass loadings and plume heights of volcanic ash clouds from satellite data, CSIROAtmosph, Res. Tech. Pap., 48, Australia, 2001.
Prata, F., Bluth, G., Rose, W., Schneider, D., and Tupper, A.: Comments on "Failures in detecting volcanic ash from a satellite-based technique", Rem. Sens. Env., 78, 341–346, 2001.
Prata, A. J. and Kerkmann, J.: Simultaneous retrieval of volcanic ash and SO2 using MSG-SEVIRI measurements, Geophys. Res. Lett., 34, L05813, doi:10.1029/2006GL028691, 2007.
Prechelt, L.: Early Stopping – but when?, in: Neural Networks: Tricks of the trade, edited by: Orr, G. and Muller, K., Springer-Heidelberg-Germany, 1998.
Pulvirenti, L., Chini, M., Pierdicca, N., Guerriero, L., and Ferrazzoli, P.: Flood monitoring us-

ing multi-temporal COSMO-SkyMed data: image segmentation and signature interpretation, Remote Sens. Environ., 115(4), 990–1002, 2011.
Sellitto, P., Solimini, D., Del Frate, F., and Casadio, S.: Tropospheric ozone column retrieval from ESA-Envisat SCIAMACHY nadir UV/VIS radiance measurements by means of a neural network algorithm, IEEE T. Geosci. Remote, under revision, 2011a.
Sellitto, P., Bojkov, B. R., Liu, X., Chance, K., and Del Frate, F.: Tropospheric ozone column retrieval from the Ozone Monitoring Instrument by means of a neural network algorithm, Atmos. Meas. Tech. Discuss., 4, 2491–2524, doi:10.5194/amtd-4-2491-2011, 2011b.
Simpson, J. J., Hufford, G. L., Pieri, D., and Berg, J. S.: Failures in detecting volcanic ash from a satellite-based technique, Remote Sens. Environ., 72, 191–217, 2000.
Simpson, J. J., Hufford, G. L., Pieri, D., and Berg, J. S.: Response to Comments on “Failures in detecting volcanic ash from a satellite-based technique”, Remote Sens. Environ.t, 78, 347–357, 2001.
Tupper, A., Carn, S., Davey, J., Kamada, Y., Potts, R., and Prata, F.: An evaluation of volcanic cloud detection techniques during recent significant eruption in the western Ring of Fire, Remote Sens. Environ., 91, 27–46, 2004.
Volz, F. E.: Infrared optical constants of ammonium sulfate, Sahara dust, volcanic pumice and fly ash, Appl. Optic., 12, 564–568, 1973.
Watson, I. M., Realmuto, V. J., Rose, W. I., Prata, A. J., Bluth, G. J. S., Gu, Y., Bader, C. E., and Yu, T.: Thermal infrared remote sensing of volcanic emissions using the moderate resolution imaging spectroradiometer, J. Volcanol. Geoth. Res., 135(1–2), 75–89, 2004.
Wen, S. and Rose, W.: Retrieval of sizes and total masses of particles in volcanic aerosol clouds using AVHRR bands 4 and 5, J. Geophys. Res., 99, 5421–5431, 1994.
Yamanouchi, T., Suzuki, K., and Kawaguchi, S.: Detection of clouds in Antarctica from infrared multispectral data of AVHRR, J. Meteo. Society of Japan, 65(6), 949–961, 1987.
Yu, T., Rose, W. I., and Prata, A. J.: Atmospheric correction for satellite-based volcanic ash mapping and retrievals using split window IR data from GOES and AVHRR, J. Geoph. Res., 107(D16), 4311, doi:10.1029/2001JD000706, 2002.

AMTD
4, 2567–2598, 2011

AMTD
4, 2567–2598, 2011

Volcanic ash monitoring from MODIS by means of NN

M. Picchiani et al.

Table 1. MODIS TIR channels characteristics.

Channel n°	Center Wavelength (µm)	NEDT (K)	Spatial Resolution (km)
28	7.3	0.25	1
29	8.5	0.05	1
30	9.7	0.25	1
31	11.0	0.05	1
32	12.0	0.05	1

Table 2. The Training, Test and Validations sets extracted from the data, for the ash detection exercise.

Data	*TrS*	*TeS*	*VeS*	Tot
28 October 2002	37416	16306	–	810000
29 October 2002	18918	8108	–	810000
30 October 2002	–	–	810000	810000
24 November 2006	–	–	810000	810000
23 July 2001	–	–	810000	810000

AMTD
4, 2567–2598, 2011

Table 3. Confusion Matrix assess the classification accuracy on the validation sets: Left column results of NN. Right column results of NN and segmentation post processing.

July 23 2001				July 23 2001			
		BTD				BTD	
		Ash	Not Ash			Ash	Not Ash
NN	Ash	8159	1163	NN	Ash	2289	201
	Not Ash	1164	799514		Not Ash	7034	800476
Overall Accuracy = 99.7 %				Overall Accuracy = 99.0 %			
K Coefficient = 0.87				K Coefficient = 0.83			
30 October 2002				30 October 2002			
		BTD				BTD	
		Ash	Not Ash			Ash	Not Ash
NN	Ash	23922	21630	NN	Ash	23755	11714
	Not Ash	565	763815		Not Ash	1164	773731
Overall Accuracy = 97.2 %				Overall Accuracy = 98.4 %			
K Coefficient = 0.67				K Coefficient = 0.78			
24 November 2006				24 November 2006			
		BTD				BTD	
		Ash	Not Ash			Ash	Not Ash
NN	Ash	2673	4833	NN	Ash	2484	397
	Not Ash	937	801468		Not Ash	1126	805904
Overall Accuracy = 99.2 %				Overall Accuracy = 99.8 %			
K Coefficient = 0.47				K Coefficient = 0.76			

AMTD
4, 2567–2598, 2011

Volcanic ash monitoring from MODIS by means of NN

M. Picchiani et al.

Table 4. The Training, Test and Validations sets for the ash mass retrieval exercise.

Data	TrS	TeS	VaS	Tot Ash	Tot
28 October 2002	11841	3634	2742	18271	810000
29 October 2002	5780	1774	1338	8892	810000
30 October 2002	8700	2670	2014	13384	810000
24 November 2006	1633	501	378	2512	160000
23 July 2001	6060	1865	1398	9323	810000

AMTD
4, 2567–2598, 2011

Table 5. The rmse values for the extracted Validations sets.

	RMSE VaS 28 October 2002	RMSE VaS 29 October 2002	RMSE VaS 30 October 2002	RMSE VaS 24 November 2006	RMSE VaS 23 July 2001
NN1: 28 October 2002	0.3756	0.5217	0.4247	0.4831	0.4032
NN2: 28 October 2002 + 29 October 2002	0.3573	0.3580	0.3408	0.4722	0.3101
NN3: 28 October 2002 + 29 October 2002 + 30 October 2002	0.4619	0.3405	0.3181	0.4712	0.2417
NN4: 28 October 2002 + 29 October 2002 + 30 October 2002 + 24 November 2006	0.4544	0.3348	0.3263	0.4528	0.2510
NN5: 28 October 2002 + 29 October 2002 + 30 October 2002 + 24 November 2006 + 23 July 2001	0.4544	0.3348	0.3263	0.4528	0.2600

AMTD
4, 2567–2598, 2011

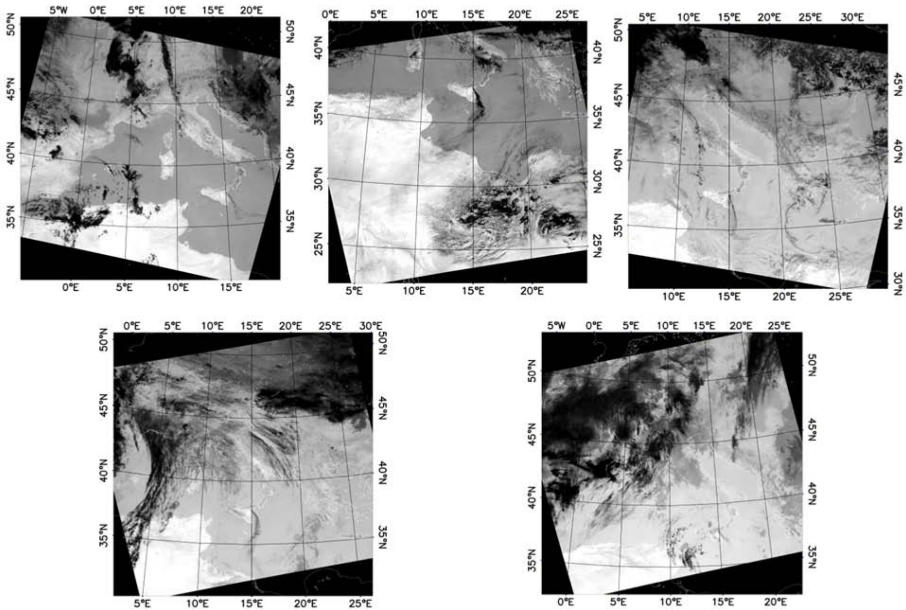

Fig. 1. MODIS test case images. Top Plates, from left to right: 23 July 2001 at 10:35 UTC; 28 October 2001 at 12:15 UTC and 29 October 2002 at 12:05 UTC. Bottom Plates, from left to right: 30 October 2002 at 9:45 UTC and 24 November 2006 at 12:20 UTC.

AMTD
4, 2567–2598, 2011

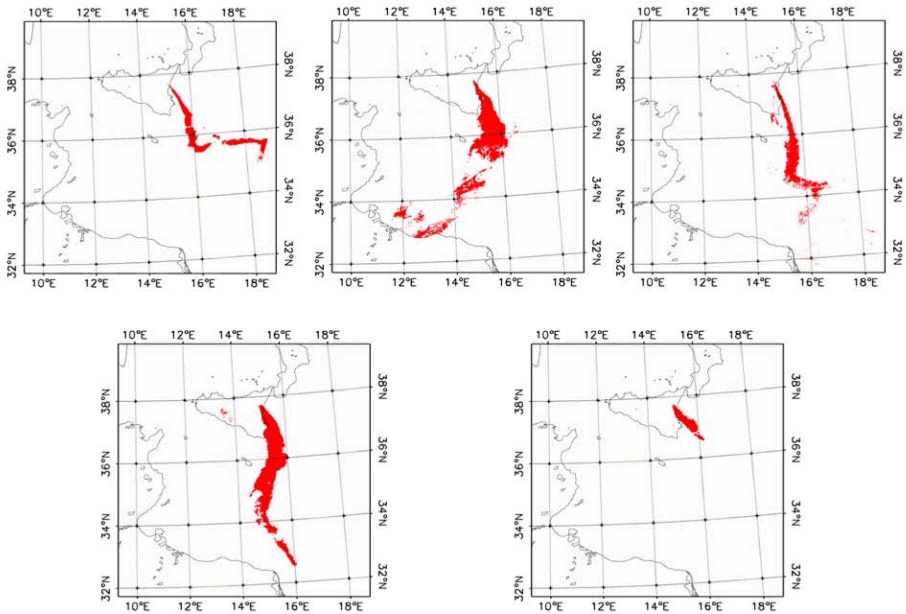

Fig. 2. MODIS BTD ash detection maps. Top Plates, from left to right: 23 July 2001, 28 October 2002 and 29 October 2002. Bottom Plates, from left to right: 30 October 2002 and 24 November 2006.

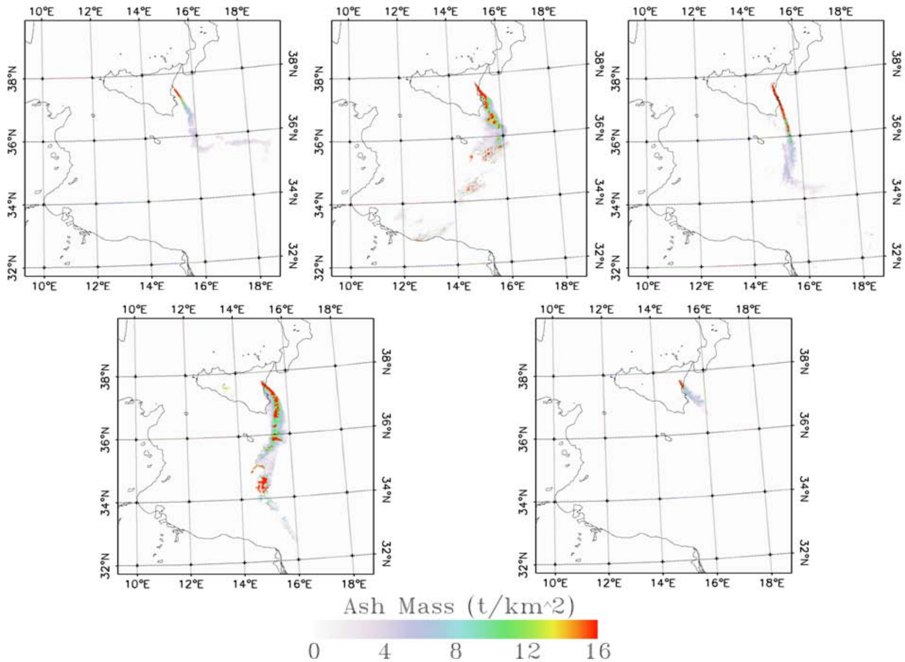

Fig. 3. MODIS BTD ash retrieval maps. Top Plates, from left to right: 23 July 2001, 28 October 2001 and 29 October 2002. Bottom Plates, from left to right: 30 October 2002 and 24 November 2006.

AMTD
4, 2567–2598, 2011

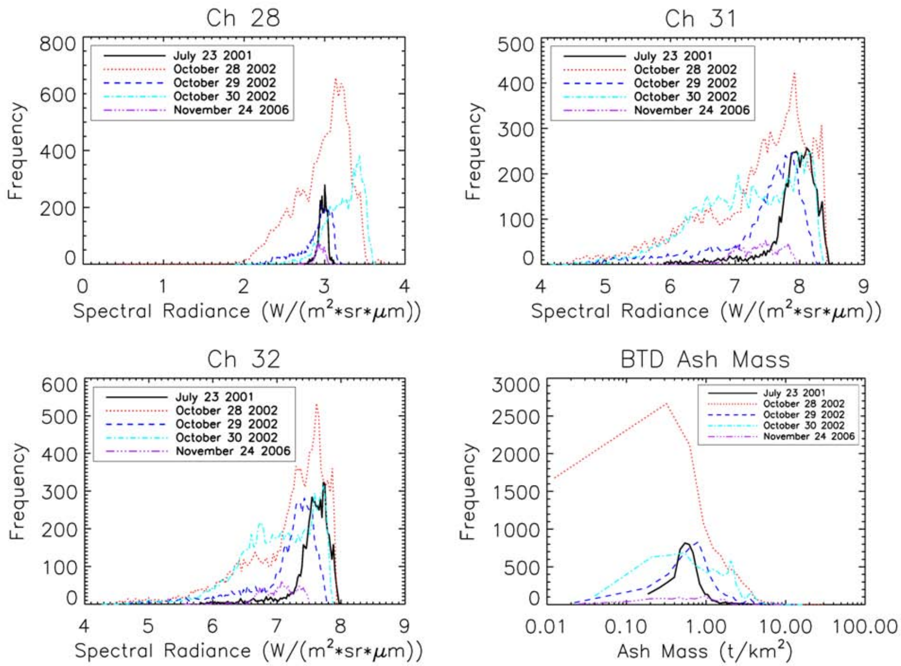

Fig. 4. The histograms computed for the three considered MODIS channels and for the BTD ash mass esteemed values, for the five considered acquisition date. Top Plates, from left to right: MODIS CH28 and CH31. Bottom Plates, from left to right: MODIS CH32 and BTD Total mass esteemed values.

AMTD
4, 2567–2598, 2011

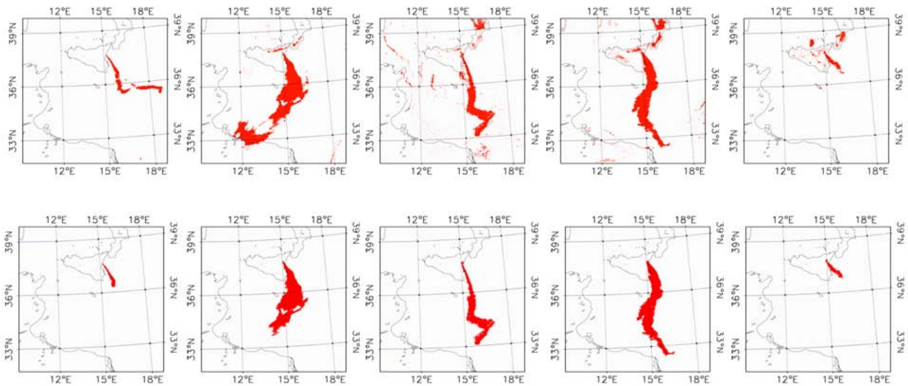

Fig. 5. MODIS NNs procedure ash maps. From left to right: 23 July 2001, 28 October 2002, 29 October 2002, 30 October 2002, and 24 November 2006. **(a)** Upper part: maps without segmentation step. **(b)** Lower part: maps with segmentation step.

AMTD
4, 2567–2598, 2011

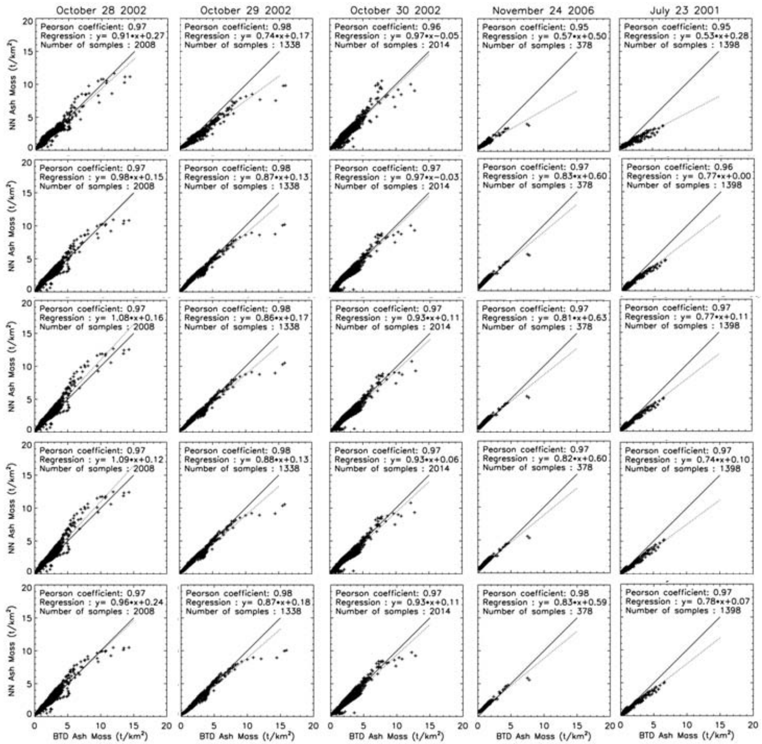

Fig. 6. Scatter plots for the five V sets, from left to right: 28 October 2002, 29 October 2002, 30 October 2002, 24 November 2006, 23 July 2001. From top to bottom results from: NN1 (28 October 2002). NN2 (28 October 2002 + 29 October 2002). NN3 (28 October 2002 + 29 October 2002 + 30 October 2002). NN4 (28 October 2002 + 29 October 2002 + 30 October 2002 + 24 November 2006). NN5 (28 October 2002 + 29 October 2002 + 30 October 2002 + 24 November 2006 + 23 July 2001).

AMTD
4, 2567–2598, 2011

Volcanic ash monitoring from MODIS by means of NN

M. Picchiani et al.

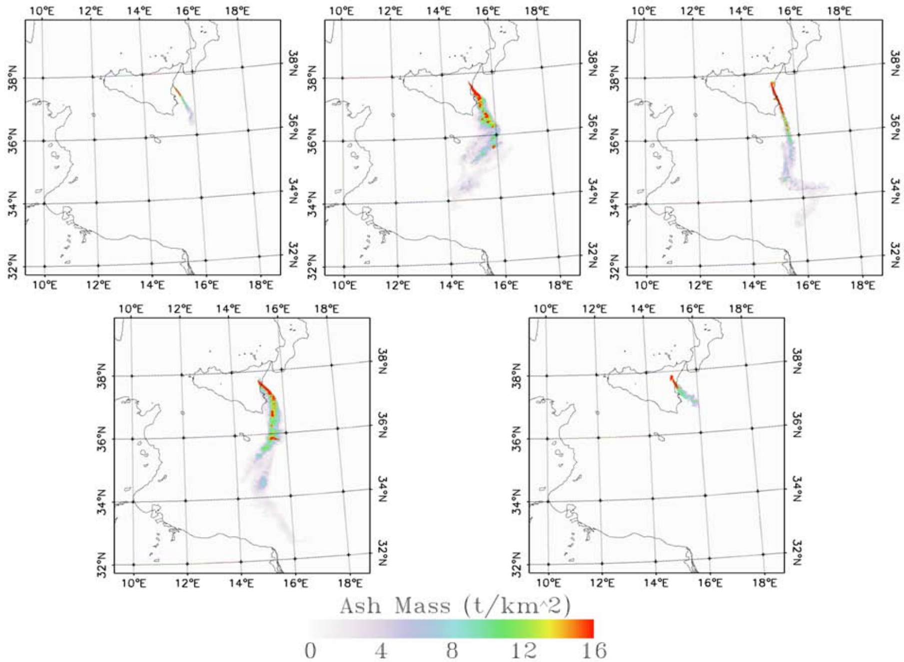

Fig. 7. NNs MODIS Ash mass maps from five different dates. Top Plates, from left to right: 23 July 2001, 28 October 2001 and 29 October 2002. Bottom Plates, from left to right: 30 October 2002 and 24 November 2006.